

ARTICLE

DOI: 10.1038/s41467-017-00069-7

OPEN

Probing ultrafast $\pi\pi^*/n\pi^*$ internal conversion in organic chromophores via K-edge resonant absorption

T.J.A. Wolf¹, R.H. Myhre^{1,2}, J.P. Cryan¹, S. Coriani^{3,4}, R.J. Squibb⁵, A. Battistoni¹, N. Berrah⁶, C. Bostedt^{7,8,9}, P. Bucksbaum^{1,10}, G. Coslovich⁷, R. Feifel⁵, K.J. Gaffney^{1,11}, J. Grilj¹², T.J. Martinez^{1,13}, S. Miyabe^{1,13,14}, S.P. Moeller⁷, M. Mucke¹⁵, A. Natan¹, R. Obaid⁶, T. Osipov⁷, O. Plekan¹⁶, S. Wang¹, H. Koch^{1,2} & M. Gühr^{1,17}

Many photoinduced processes including photosynthesis and human vision happen in organic molecules and involve coupled femtosecond dynamics of nuclei and electrons. Organic molecules with heteroatoms often possess an important excited-state relaxation channel from an optically allowed $\pi\pi^*$ to a dark $n\pi^*$ state. The $\pi\pi^*/n\pi^*$ internal conversion is difficult to investigate, as most spectroscopic methods are not exclusively sensitive to changes in the excited-state electronic structure. Here, we report achieving the required sensitivity by exploiting the element and site specificity of near-edge soft X-ray absorption spectroscopy. As a hole forms in the n orbital during $\pi\pi^*/n\pi^*$ internal conversion, the absorption spectrum at the heteroatom K-edge exhibits an additional resonance. We demonstrate the concept using the nucleobase thymine at the oxygen K-edge, and unambiguously show that $\pi\pi^*/n\pi^*$ internal conversion takes place within (60 ± 30) fs. High-level-coupled cluster calculations confirm the method's impressive electronic structure sensitivity for excited-state investigations.

¹Stanford PULSE Institute, SLAC National Accelerator Laboratory, 2575 Sand Hill Road, Menlo Park, CA 94025, USA. ²Department of Chemistry, Norwegian University of Science and Technology, NO-7491 Trondheim, Norway. ³Dipartimento di Scienze Chimiche e Farmaceutiche, Università degli Studi di Trieste, Piazzale Europa 1, Trieste IT-34127, Italy. ⁴Department of Chemistry, Technical University of Denmark, 2800 Kongens Lyngby, Denmark. ⁵Department of Physics, University of Gothenburg, SE-412 96 Gothenburg, Sweden. ⁶Department of Physics, University of Connecticut, 2152 Hillside Road, Storrs, CT 06269, USA. ⁷Linac Coherent Light Source, SLAC National Accelerator Laboratory, 2575 Sand Hill Road, Menlo Park, CA 94025, USA. ⁸Argonne National Laboratory, 9700 Cass Avenue, Lemont, IL 60439, USA. ⁹Department of Physics and Astronomy, Northwestern University, 2145 Sheridan Road, Evanston, IL 60208, USA. ¹⁰Department of Physics, Stanford University, 382 Via Pueblo Mall, Stanford, CA 94305, USA. ¹¹Stanford Synchrotron Radiation Lightsource, SLAC National Accelerator Laboratory, 2575 Sand Hill Road, Menlo Park, CA 94025, USA. ¹²Laboratory of Ultrafast Spectroscopy, Ecole Polytechnique Federal de Lausanne, Lausanne CH-1015, Switzerland. ¹³Department of Chemistry, Stanford University, 333 Campus Drive, Stanford, CA 94305, USA. ¹⁴Laser Technology Laboratory, RIKEN, Wako, Saitama 351-0198, Japan. ¹⁵Department of Physics and Astronomy, Uppsala University, Box 516, SE-751 20 Uppsala, Sweden. ¹⁶Elettra-Sincrotrone Trieste, Strada Statale 14-km 163,5 AREA Science Park, IT-34149 BasovizzaTrieste, Italy. ¹⁷Institut für Physik und Astronomie, Universität Potsdam, Karl-Liebknecht-Straße 24/25, DE-14476 Potsdam, Germany. Correspondence and requests for materials should be addressed to H.K. (email: henrik.koch@ntnu.no) or to M.G. (email: mguehr@uni-potsdam.de)

The efficient conversion of light into other forms of energy has a key role in many processes such as photosynthesis or human vision^{1,2}. It is well established that the efficiency of these processes is facilitated by coupled ultrafast electronic and nuclear dynamics that cannot be described using the Born–Oppenheimer approximation (BOA). The breakdown of the BOA makes the fundamental details of such mechanisms notoriously difficult to understand: they proceed on ultrafast timescales and occur mostly at positions where potential energy surfaces come close or even intersect. From an experimental point of view, it is highly desirable to access the nuclear geometry and the electronic degrees of freedom separately, to compare them to quantum simulations. The transient nuclear geometry can be best studied by time-resolved diffraction techniques using short X-ray^{3,4} or electron pulses⁵.

X-ray absorption spectroscopy has been known for a long time to be an element and site-specific probe for local electronic structure of organic molecules and the charge states and local environment of transition metal sites⁶. The element and site specificity originates from excitation of inner electrons, which are strongly confined around the specific nucleus, into empty valence molecular orbitals. As the core electron energy levels often lie 10s and 100s of eVs apart, a specific site in a molecule can be probed by selection of the incident photon energy. Fueled by the development of short X-ray pulse sources⁷ and the growing interest in transition metal-based photocatalysts and photosensitizers, transient X-ray spectroscopy was very successfully applied to the K- and L-edges of the active transition metal centers in those compounds^{8–11}. These studies showed an impressive sensitivity to transiently populated electronic states involving the metal center, e.g., metal-to-ligand charge transfer (MLCT) states.

Internal conversion between excited states of different electronic character is also a crucial path for photoenergy conversion in organic molecules. Organic chromophores exhibit strongly absorbing $\pi\pi^*$ excited states, which can be described in a single

electron Hartree–Fock (HF) picture as an electron–hole pair in a formerly occupied and an unoccupied molecular orbital (MO), both with π symmetry. Many of these chromophores, like azo-switches^{12,13}, nucleobases^{14–16}, and amino acids¹⁷, also contain heteroatoms with electron lone pairs. They therefore exhibit $n\pi^*$ excited states, with a hole in a heteroatom-centered lone pair (n) orbital and an electron in a π^* orbital. Unlike $\pi\pi^*$ excited states, $n\pi^*$ states are usually not directly accessible because of low absorption cross-sections from the ground state. It is therefore crucial to directly monitor the $\pi\pi^*/n\pi^*$ internal conversion as it provides essential photochemical pathways for reactions like *cis-trans* isomerization, and intersystem crossing to the triplet manifold of electronic states governed by the El Sayed selection rules¹⁸.

The preferential localization of the n orbital at the heteroatom has wide-reaching implications for resonant core level spectroscopy. In general, near edge X-ray absorption fine structure (NEXAFS) spectra show isolated features from resonant states below the core ionization edge of an element. Those features are because of transitions from this element's core orbital to unoccupied valence orbitals, e.g., a π^* orbital. The core-to-valence absorption cross-section is strongly dependent on the spatial overlap between the confined core and the empty valence orbital^{6,19,20} (Fig. 1a). In the case of excited states, the electron hole in a formerly occupied valence orbital enables an additional NEXAFS resonance. The spatial overlap makes a $1s-n$ transition from the strongly localized heteroatom $1s$ core level to the electron hole of an $n\pi^*$ state more intense than the $1s-\pi$ transition to the delocalized π hole of a $\pi\pi^*$ state. The same effect is observable in the strong sensitivity of time-resolved (TR) NEXAFS spectroscopy to MLCT states in transition metal complexes. The TR-NEXAFS signature from a photoexcited $\pi\pi^*$ state is therefore expected to be weak and to transform into a strong $n\pi^*$ -state signature as the molecule undergoes $\pi\pi^*/n\pi^*$ internal conversion, largely independent of geometry changes during the dynamics.

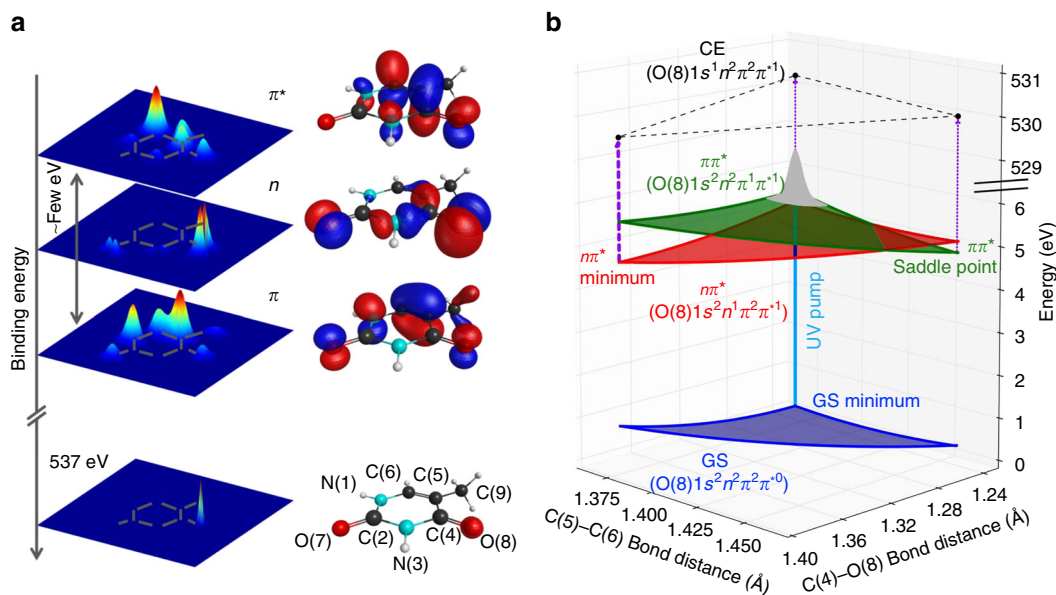


Fig. 1 Excited states of thymine and their electronic characters. **a** Isosurface representations (right) and electron density projections onto the molecular plane for the three valence orbitals (Hartree–Fock/6-311 G) involved in the characters of the two lowest lying excited states of thymine and a core orbital localized at oxygen(8). The electron density at the position of the core orbital differs strongly for the different valence orbitals. **b** Results from our coupled cluster investigation of the excited-state topology along the two most relevant degrees of freedom for relaxation into the $n\pi^*$ minimum. All states are labeled with their electron configuration. Ultraviolet (UV) excitation of the ground state (GS) places a nuclear wavepacket (gray) on the $\pi\pi^*$ excited state. It relaxes through a conical intersection to a minimum in the $n\pi^*$ excited state. According to our calculations, only one core-excited state (CE) characterized by an excitation at O(8) is relevant for interpretation of our experimental results

One benchmark molecule for the sensitivity of TR-NEXAFS spectroscopy to the $\pi\pi^*/n\pi^*$ transition is the chromophore thymine, as there is a rich literature on its excited states (see^{14, 15, 21} and citations therein). Thymine exhibits two high-lying occupied MOs, an oxygen-localized n -orbital and a delocalized π -orbital (Fig. 1a). Its lowest unoccupied MO (π^*) is similar to the π MO in delocalization. The molecule can be excited at 267 nm to a $\pi\pi^*$ state; the lower-lying $n\pi^*$ state is optically dark.

The $\pi\pi^*$ relaxation in thymine has been experimentally investigated using many methods available in ultrafast technology^{14, 15, 21} including our own study, where we investigated excited-state nonresonant Auger spectra at the oxygen K-edge²². It is challenging to attribute the experimental signatures of sub-100 fs thymine dynamics from ultrafast photoelectron¹⁶, photoion²³, absorption, or Auger electron spectroscopy²² unambiguously to a particular process, like internal conversion, as changes in both the electronic structure and the nuclear geometry influence the observables. Interpretations of past experimental data involving valence electrons relied heavily on simulations. However, theoretical investigations do not agree on a common prediction of the excited-state dynamics¹⁴. Several wavepacket

simulations predict nuclear relaxation into a local minimum of the $\pi\pi^*$ state within 100 fs followed by slower $\pi\pi^*/n\pi^*$ ^{24, 25} or even $\pi\pi^*/\text{ground state}$ ²⁶ internal conversion over a barrier. Others predict barrierless, sub-100 fs $\pi\pi^*/n\pi^*$ relaxation²⁷ or direct $\pi\pi^*/\text{ground-state}$ relaxation within few hundred fs²⁸. It is therefore unclear, if and on which timescale the $n\pi^*$ state is accessed during the relaxation dynamics.

In this work, we demonstrate application of the well-established state sensitivity of transition metal X-ray absorption spectroscopy to time resolved spectroscopy of electronic relaxation in organic molecules, closing an important gap in the photochemistry that can be investigated. We demonstrate at the example of thymine that our TR-NEXAFS technique is strongly and selectively sensitive to the ultrafast $\pi\pi^*/n\pi^*$ internal conversion. We prove the existence of the relaxation channel into the $n\pi^*$ state, its ultrafast population and depopulation. Employing computationally demanding, but quantitative high-level-coupled cluster (CC) simulations^{29–31}, which are still unavailable for transition metal complexes, we confirm our spectroscopic attribution based on orbital localization.

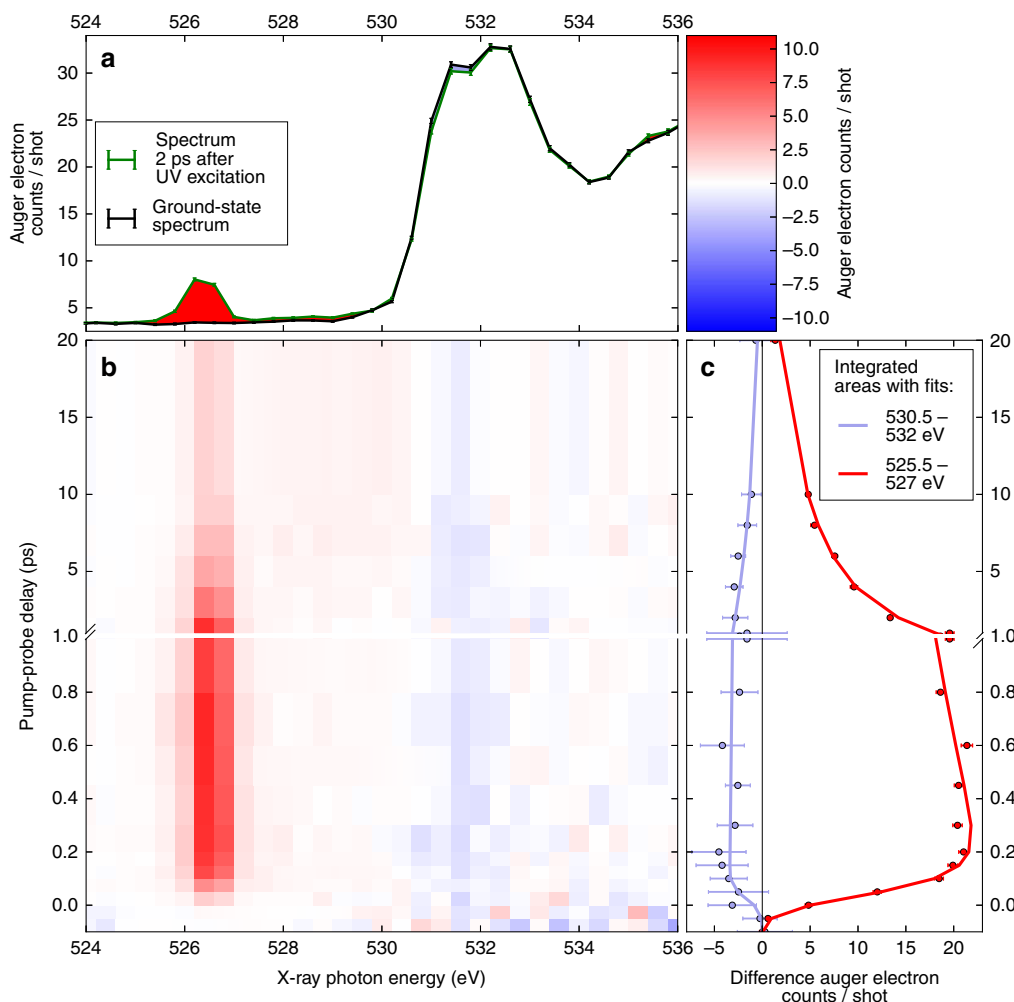


Fig. 2 Transient oxygen-edge absorption spectra of thymine. **a** Representative near-edge absorption fine structure (NEXAFS) spectra 2 ps after ultraviolet (UV) excitation and without UV excitation. UV-induced increase in intensity is marked red, UV-induced decrease is light blue. UV excitation leads to the appearance of a new spectral feature around 526.4 eV and a bleach of the ground state π^* resonance at 531.4 eV. **b** False-color plot of time-dependent NEXAFS difference spectra (see color bar in the upper right corner). The UV-induced features at 526.4 and 531.4 eV are clearly visible throughout the positive pump-probe delays. **c** Time-dependence of the UV-induced features with fits based on a rate equation model. All error bars represent the standard error of mean

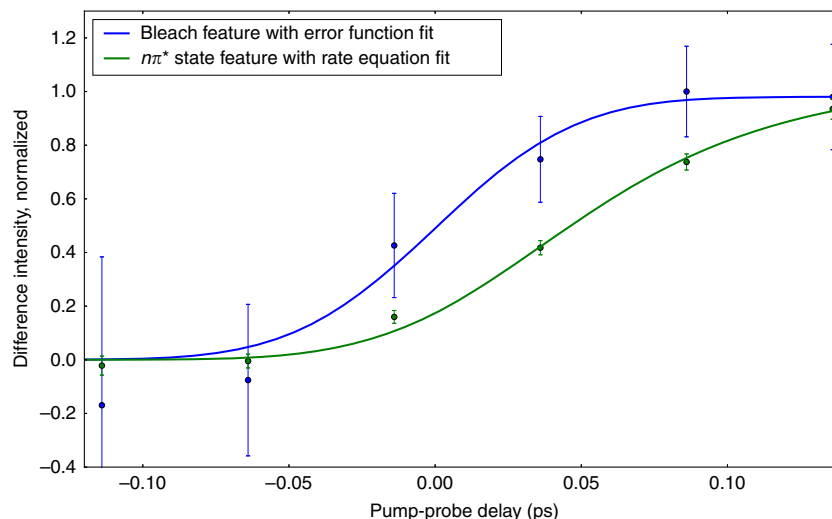


Fig. 3 Delay between the onsets of ground-state bleach and excited-state signature. The experimental data for the bleach signal (blue) are extracted from a region of interest in the Auger spectra from the photon energy region, where the bleach is observable in the near-edge absorption fine structure spectra. For better comparison with the corresponding data set from the region of the $n\pi^*$ feature (green), the bleach data set is inverted. Both data sets are normalized to the maximum modulation. The time-dependence of the $n\pi^*$ feature is fitted with the rate equation model. The delay between the bleach and the $n\pi^*$ feature is clearly visible. All error bars represent the standard error of mean

Results

Ground-state and excited-state NEXAFS spectra. The experimental ground-state NEXAFS spectrum of thymine is shown in black in Fig. 2a. It exhibits a double peak π^* resonance. On the basis of our CC calculations, and in agreement with earlier studies³², we assign the lower energy peak at 531.4 eV to a linear combination of HF single electron excitations from the O(8) 1s orbital to several unoccupied π^* orbitals with significant contributions from the aforementioned π^* MO. The linear combination is such that the core excited state possesses a high degree of electron localization at O(8), thus the strong absorption cross-section in the Mbarn regime (see a discussion in Supplementary Note 1 and Supplementary Fig. 1). The higher energy peak at 532.2 eV corresponds to an excitation from the O(7) 1s orbital to a different linear combination of π^* MOs³². The increase in intensity at photon energies beyond the π^* resonances is predominantly because of a smooth feature of K-edge ionization at 537 eV and additional weak resonant transitions³².

The NEXAFS spectrum taken 2 ps after ultraviolet (UV) excitation is shown in green in Fig. 2a. It is a superposition of the excited-state spectrum and the ground-state spectrum, which is weakened by transfer of an estimated 13% of the population (Supplementary Notes 2–4) to the excited state. The excited-state spectrum is redshifted to lower photon energies with respect to the ground state, which is obvious by the background-free signature at 526.4 eV. This signature must be a new core excitation channel either to the n or π electron hole. An additional signature of UV excitation, the intensity reduction in the area of the π^* resonances, is the result of a bleach of the ground-state spectrum almost entirely compensated by the redshift of the smooth K-edge ionization feature in the excited-state spectrum. The effect is therefore only visible, where the ground state exhibits the strongest intensity modulations, i.e., the π^* resonance. It is therefore a direct signature of the ground-state depopulation and largely independent of any following excited-state dynamics.

Signature of ultrafast $\pi\pi^*/n\pi^*$ internal conversion. The time-dependence of the difference signal (X-ray absorption with UV

minus X-ray absorption without UV) is shown in Fig. 2b. The spectrally integrated time trends of the ground-state bleach and excited-state feature are shown in Fig. 2c. The temporal onset of the excited-state feature exhibits a delay ((60 ± 30) fs according to a rate equation fit, see Supplementary Note 2) with respect to the temporal overlap between UV and X-ray pulses, which is marked by the bleach onset. To confirm the fit of the rather noisy bleach feature, we defined a narrower integration region in the Auger spectra based on best signal to noise for the bleach feature. The resulting curves and fits are shown in Fig. 3. The intensity of the 526.4 eV feature is only because of 13% of the population in the ground-state NEXAFS spectrum. Its absorption cross-section is, thus, similar to the π^* resonance. Therefore, it must be likewise due to a localized transition, which is the signature of the $n\pi^*$ state, not the $\pi\pi^*$ state. Accordingly, the delay of the $n\pi^*$ signature of (60 ± 30) fs directly reflects the nuclear wavepacket dynamics to access the $\pi\pi^*/n\pi^*$ conical intersection seam, in agreement with a short $\pi\pi^*$ lifetime observed in our earlier study²². Our intuitive interpretation is supported by our CC investigations of the $\pi\pi^*$ and $n\pi^*$ -state potential energy surfaces. Figure 1b shows a reduced potential energy sketch from our simulations along the two nuclear coordinates, which are expected to be most relevant for the molecular dynamics. We could not observe any accessible local minima in the $\pi\pi^*$ state and instead found the $\pi\pi^*/n\pi^*$ conical intersection seam not to be isolated by a barrier from the Franck–Condon (FC) point, but directly accessible. This suggests that after photoexcitation, the nuclear wavepacket is driven out of the FC region by a gradient along the C(5)–C(6) bond elongation towards a saddle point. On its way, it encounters the $\pi\pi^*/n\pi^*$ conical intersection seam, which is in agreement with the experimentally observed internal conversion on a sub-100 fs timescale. In the $n\pi^*$ excited state, a local minimum can be reached from the $\pi\pi^*/n\pi^*$ conical intersection by O(8)–C(4) bond elongation³³.

We, furthermore, performed CC simulations of NEXAFS spectra of the ground state, and of the excited states at the minimum and saddle point geometries identified in Fig. 1b. Figure 4 shows a comparison of calculated to experimental spectra of the ground state and 2 ps after UV excitation. All three simulated excited-state spectra exhibit their lowest-energy resonance around 526.4 eV. In all cases, the final state is the

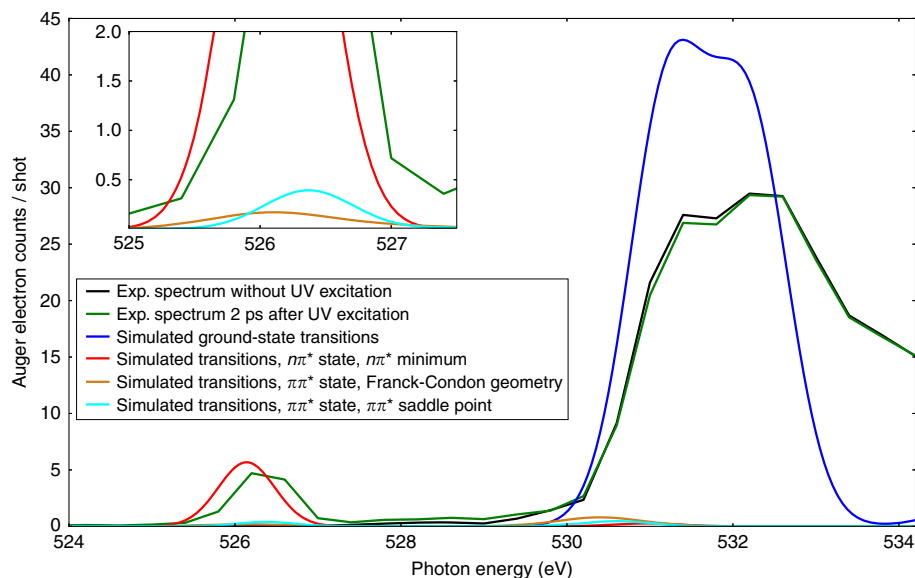


Fig. 4 Comparison of experimental and simulated spectra. Simulated near-edge absorption fine structure spectra of the ground state, the $\pi\pi^*$ state in the Franck-Condon region and at the saddle point, and the $n\pi^*$ state at its minimum. For comparison, the experimental ground-state spectrum and the experimental spectrum 2 ps after ultraviolet (UV) excitation are shown. Relative intensities of simulated and experimental ground-state spectra are adjusted to an equal peak area of the π^* resonances. Simulated excited-state spectra are scaled with respect to the ground-state spectrum assuming 13% excitation. The *inset* shows a detailed view of the intensity relations at the position of the excited-state feature. Contributions from K-edge ionization were not included in the simulations

same O(8)-centered core-excited state (CE). As expected, the oscillator strength in the $n\pi^*$ state beats the $\pi\pi^*$ state by a factor of 40, almost independent of the molecular geometry (Supplementary Tables 1–3). We scaled the simulated excited-state spectra to the estimated ratio of 13% excited molecules. Only the simulated $n\pi^*$ -state spectrum shows a comparable intensity at the 526.4 eV position.

Discussion

With the TR-NEXAFS method presented here, we can confirm population of the $n\pi^*$ state through a directly accessible conical intersection within 60 fs. Comparison of experimentally observed and calculated NEXAFS absorption intensities suggests that internal conversion into the $n\pi^*$ state is a major channel in the relaxation dynamics of thymine (Supplementary Note 3).

An alternative method to explore the electronic relaxation, however less selectively sensitive to electronic structure changes, is time-resolved photoelectron spectroscopy using extreme ultraviolet pulses³⁴. Here one relies on spectrally resolving ionic continua that single out certain valence states³⁵, thus exhibiting nonadiabatic transitions by kinetic energy or angular distribution changes^{36, 37}. An assignment is, however, only possible by high-level simulations of excited-state ionization cross-sections, whereas we confirm the validity of our intuitive orbital-based assignment of core excitations by quantitative CC simulations.

The $n\pi^*$ signature in our TR-NEXAFS spectra shows a biexponential decay with time constants of (1.9 ± 0.1) ps and (10.5 ± 0.2) ps. This supports a consecutive relaxation process via a level with $n\pi^*$ character to a final level of non- $n\pi^*$ character, to which our method is insensitive. The $n\pi^*$ level is most probably another minimum in the singlet $n\pi^*$ state, as intersystem crossing to a triplet $n\pi^*$ state is forbidden by the El Sayed selection rule. The transition to the final state can be either intersystem crossing to a nearby triplet $\pi\pi^*$ state with strong spin orbit coupling³⁸ or internal conversion to the ground state³⁹, which is supported by

the recovery of the ground-state bleach in our data. Recent simulations on ethylene⁴⁰ suggest that $1s-\pi$ absorption lines exhibit geometry-dependent line shifts. We predicted those features to be relatively weak in the case of thymine, especially at the oxygen K-edge. It would be exciting to explore this opportunity in a future experiment with sufficient signal to noise. In a similar way, a recent study on time resolved absorption spectroscopy at the carbon K-edge uses symmetry effects on the X-ray absorption spectrum to probe strong field induced dissociation of SF₆⁴¹. This is particularly exciting taking into account that a high harmonic source was used to accomplish this.

In conclusion, we demonstrate with this work the application of time-resolved X-ray absorption spectroscopy to organic molecules containing heteroatoms with lone pairs to selectively investigate ultrafast $\pi\pi^*/n\pi^*$ internal conversion, a crucial mechanistic step in this large class of molecules. We use the dominating absorption strength of the heteroatom $1s-n$ resonance to directly monitor this nonadiabatic process. Our results prove that the method already works reliably under the current, still challenging conditions of X-ray free-electron laser experiments with low repetition rates and high temporal and spectral jitter. Application of the method is in principle not confined to the gas phase. A soft X-ray study of molecular desorption using similar technical constraints but different molecular processes has been already performed at surfaces⁴². In addition, recently developed liquid sheets allow for time-resolved solution studies in the water window⁴³. Our approach has the potential to become a standard tool for ultrafast investigations at the upcoming second generation of ultrafast X-ray sources, which provide the opportunity to extend the TR-NEXAFS technique towards multi-dimensional spectroscopy approaches in the soft X-ray regime⁴⁴.

Methods

Experimental methods. The experiment was performed at the Linac Coherent Light Source (LCLS) free electron laser (FEL) facility, SLAC National Accelerator Laboratory, at the soft X-ray (SXR) instrument^{7, 45}. A schematic representation of

the experimental setup is shown in Supplementary Fig. 2. Thymine was purchased from Sigma Aldrich and evaporated by an effusive oven into an ultra high vacuum chamber at a temperature of 160°C leading to a sample density of 10^{12} cm^{-3} in the overlap region of optical and X-ray laser^{22, 46}. Molecules were excited by 267 nm pulses with 70 fs duration and a focus diameter of 100 μm full width at half maximum (FWHM). Soft X-ray pulses with 70 fs duration and a focus diameter of 70 μm FWHM were used to probe the sample in the oxygen K-edge spectral region from 520 to 550 eV by simultaneously tuning the FEL and the monochromator of the SXR instrument with an energy resolution of $<0.5 \text{ eV}$ ⁴⁷. The intensity of the essentially background-free transient feature at 526.4 eV was measured for a wide range of UV pump intensities, to make sure the experiment took place in the linear absorption regime well below saturation (Supplementary Fig. 3). Temporal and spatial overlap of UV and SXR pulses was optimized to bleach the Auger spectra of thymine which is induced by photofragmentation at high UV intensities. Oxygen 1s Auger spectra were recorded with the 2 m long LCLS-FELCO (LCLS-FEL correlation) magnetic bottle spectrometer⁴⁸. The photon energy-dependent absorption cross-section of the sample is proportional to the integrated Auger electron yield. SXR pulses were delayed with respect to UV pulses between -200 fs and 20 ps . To achieve NEXAFS difference spectra, UV laser pulses were blocked on a shot-by-shot basis. LCLS pulses are strongly fluctuating in intensity and relative arrival time. Therefore, both parameters were recorded on a shot-by-shot basis by an optical X-ray cross-correlator⁴⁹ and a gas detector after the monochromator, respectively. The data set was resorted into $\geq 50 \text{ fs}$ delay bins and several X-ray intensity bins. Difference spectra from different X-ray intensity bins were averaged.

Theoretical methods. The thymine ground-state geometry (Supplementary Table 4) was optimized with CCSD(T)/aug-cc-pVDZ using CFOUR⁵⁰. Excited-state geometries (Supplementary Tables 5 and 6) were optimized at the EOM-CCSD/aug-cc-pVDZ level employing Q-Chem⁵¹. No symmetry restrictions were applied for geometry optimizations. Valence excitation energies were obtained with CC3 using the aug-cc-pVDZ basis on the oxygen atoms and the aug-cc-pVDZ basis on the other atoms (Supplementary Table 7). We employed a newly developed implementation in Dalton^{29, 52–54}. Oxygen 1s to valence excitation energies and oscillator strengths were computed at the CCSD level of theory with the same basis as for the valence excitations using a newly developed linear response code employing the core-valence separation (CVS) approximation and implemented in Dalton^{31, 55–57} (Supplementary Tables 1–3). This procedure has previously been shown to be highly accurate within the coupled cluster hierarchy of methods. In the CVS approximation, we excluded the pure valence excitations and require the excitation operators to include at least one core orbital—in this way the excitation energies for core-excited states become the lowest eigenvalues of the coupled cluster response matrix. Transition moments are calculated using coupled cluster response theory for transitions between excited states. The core to valence excitation energies was offset-corrected by benchmark calculations of the lowest core to valence excitation energies at the CC3/aug-cc-pCVTZ/aug-cc-pVDZ level (Supplementary Table 8). With this correction, we achieve quantitative agreement with the NEXAFS transition energies within the experimental error bars on a purely ab initio basis. The theoretical core excitation energies are not corrected for relativistic effects and we estimate the effect to increase excitation energies by 0.1–0.3 eV.

Thymine exhibits C_s symmetry in the ground state. The two lowest-lying excited states have different representations, $A'(n\pi^*)$ and $A''(\pi\pi^*)$, and the $\pi\pi^*/n\pi^*$ conical intersection is symmetry allowed. We note that no complex eigenvalues of the Jacobian matrix were encountered in the vicinity of the conical intersection seam⁵⁸. In contrast to earlier studies^{24–26}, we could not identify a minimum in the $\pi\pi^*$ state. Instead, we found a saddle point geometry with C_s symmetry, which is directly accessible from the Franck–Condon region. The energy lowering degrees of freedom of the saddle point are out of plane bending, as confirmed by frequency calculations, which were performed for all observed stationary points^{59, 60} (Supplementary Tables 9–11). The $n\pi^*$ minimum geometry is distorted from C_s symmetry with O(8) out of the plane. We encountered the $\pi\pi^*/n\pi^*$ conical intersection seam in between the Franck–Condon point and the $\pi\pi^*$ saddle point in close proximity to the latter (energy difference $<0.03 \text{ eV}$). On the basis of calculated core excitation energies and oscillator strengths, NEXAFS spectra were simulated by convoluting theoretical stick spectra with Gaussians to account for peak broadening and the experimental energy resolution.

Data availability. The data sets generated during and/or analyzed during the current study are available from the corresponding authors on reasonable request.

Received: 7 March 2017 Accepted: 28 April 2017

Published online: 22 June 2017

References

- Cheng, Y.-C. & Fleming, G. R. Dynamics of light harvesting in photosynthesis. *Annu. Rev. Phys. Chem.* **60**, 241–262 (2009).
- Polli, D. *et al.* Conical intersection dynamics of the primary photoisomerization event in vision. *Nature* **467**, 440–443 (2010).
- Minitti, M. P. *et al.* Imaging molecular motion: femtosecond X-ray scattering of an electrocyclic chemical reaction. *Phys. Rev. Lett.* **114**, 255501 (2015).
- Küpper, J. *et al.* X-ray diffraction from isolated and strongly aligned gas-phase molecules with a free-electron laser. *Phys. Rev. Lett.* **112**, 83002 (2014).
- Yang, J. *et al.* Diffractive imaging of a rotational wavepacket in nitrogen molecules with femtosecond mega-electronvolt electron pulses. *Nat. Commun.* **7**, 11232 (2016).
- Stöhr, J. *NEXAFS Spectroscopy*. (Springer, 1996).
- Emma, P. *et al.* First lasing and operation of an angstrom-wavelength free-electron laser. *Nat. Photonics* **4**, 641–647 (2010).
- Bressler, C. & Chergui, M. Molecular structural dynamics probed by ultrafast X-ray absorption spectroscopy. *Annu. Rev. Phys. Chem.* **61**, 263–282 (2010).
- Wernet, P. *et al.* Orbital-specific mapping of the ligand exchange dynamics of $\text{Fe}(\text{CO})_5$ in solution. *Nature* **520**, 78–81 (2015).
- Zhang, W. *et al.* Tracking excited-state charge and spin dynamics in iron coordination complexes. *Nature* **509**, 345–348 (2014).
- Chen, L. X. in *X-Ray Absorption and X-Ray Emission Spectroscopy: Theory and Applications* (eds Bokhoven, J. A. V. & Lamberti, C.) 213–249 (John Wiley & Sons, Ltd, 2016).
- Comstock, M. *et al.* Reversible photomechanical switching of individual engineered molecules at a metallic surface. *Phys. Rev. Lett.* **99**, 38301 (2007).
- Hosono, N. *et al.* Large-area three-dimensional molecular ordering of a polymer brush by one-step processing. *Science* **330**, 808–811 (2010).
- Improta, R., Santoro, F. & Blancafort, L. Quantum mechanical studies on the photophysics and the photochemistry of nucleic acids and nucleobases. *Chem. Rev.* **116**, 3540–3593 (2016).
- Middleton, C. T. *et al.* DNA excited-state dynamics: from single bases to the double helix. *Annu. Rev. Phys. Chem.* **60**, 217–239 (2009).
- Ullrich, S., Schultz, T., Zgierski, M. Z. & Stolow, A. Electronic relaxation dynamics in DNA and RNA bases studied by time-resolved photoelectron spectroscopy. *Phys. Chem. Chem. Phys.* **6**, 2796–2801 (2004).
- Klessinger, M. & Michl, J. *Excited States and Photochemistry of Organic Molecules*. (Wiley, 1995).
- El Sayed, M. A. Spin–orbit coupling and the radiationless processes in nitrogen heterocycles. *J. Chem. Phys.* **38**, 2834–2838 (1963).
- Manne, R. Molecular orbital interpretation of X-ray emission spectra: simple hydrocarbons and carbon oxides. *J. Chem. Phys.* **52**, 5733–5739 (1970).
- Ueda, K. High-resolution inner-shell spectroscopies of free atoms and molecules using soft-X-ray beamlines at the third-generation synchrotron radiation sources. *J. Phys. B At. Mol. Opt. Phys.* **36**, R1–R47 (2003).
- Kleiner, K., Nachtigallová, D. & de Vries, M. S. Excited state dynamics of DNA bases. *Int. Rev. Phys. Chem.* **32**, 308–342 (2013).
- McFarland, B. K. *et al.* Ultrafast X-ray Auger probing of photoexcited molecular dynamics. *Nat. Commun.* **5**, 4235 (2014).
- Kang, H., Lee, K. T., Jung, B., Ko, Y. J. & Kim, S. K. Intrinsic lifetimes of the excited state of DNA and RNA bases. *J. Am. Chem. Soc.* **124**, 12958–12959 (2002).
- Hudock, H. R. *et al.* Ab initio molecular dynamics and time-resolved photoelectron spectroscopy of electronically excited uracil and thymine. *J. Phys. Chem. A* **111**, 8500–8508 (2007).
- Barbatti, M. *et al.* Relaxation mechanisms of UV-photoexcited DNA and RNA nucleobases. *Proc. Natl Acad. Sci.* **107**, 21453–21458 (2010).
- Asturiol, D., Lasorne, B., Robb, M. A. & Blancafort, L. Photophysics of the $\pi\pi^*$ and $n\pi^*$ states of thymine: MS-CASPT2 minimum-energy paths and CASSCF on-the-fly dynamics. *J. Phys. Chem. A* **113**, 10211–10218 (2009).
- Picconi, D., Barone, V., Lami, A., Santoro, F. & Improta, R. The interplay between $\pi\pi^*/n\pi^*$ excited states in gas-phase thymine: a quantum dynamical study. *ChemPhysChem* **12**, 1957–1968 (2011).
- Nakayama, A., Arai, G., Yamazaki, S. & Taketsugu, T. Solvent effects on the ultrafast nonradiative deactivation mechanisms of thymine in aqueous solution: excited-state QM/MM molecular dynamics simulations. *J. Chem. Phys.* **139**, 214304 (2013).
- Myhre, R. H. & Koch, H. The multilevel CC3 coupled cluster model. *J. Chem. Phys.* **145**, 44111 (2016).
- Bartlett, R. J. & Musiał, M. Coupled-cluster theory in quantum chemistry. *Rev. Mod. Phys.* **79**, 291–352 (2007).
- Coriani, S. & Koch, H. Communication: x-ray absorption spectra and core-ionization potentials within a core-valence separated coupled cluster framework. *J. Chem. Phys.* **143**, 181103 (2015).
- Plekan, O. *et al.* A theoretical and experimental study of the near edge X-ray absorption fine structure (NEXAFS) and X-ray photoelectron spectra (XPS) of nucleobases: thymine and adenine. *Chem. Phys.* **347**, 360–375 (2008).
- Yamazaki, S. & Taketsugu, T. Nonradiative deactivation mechanisms of uracil, thymine, and 5-fluorouracil: a comparative ab initio study. *J. Phys. Chem. A* **116**, 491–503 (2012).
- Koch, M., Wolf, T. J. A. & Gühr, M. Understanding the modulation mechanism in resonance-enhanced multiphoton probing of molecular dynamics. *Phys. Rev. A* **91**, 031403(R) (2015).

35. Blanchet, V., Zgierski, M. Z., Seideman, T. & Stolow, A. Discerning vibronic molecular dynamics using time-resolved photoelectron spectroscopy. *Nature* **401**, 52–54 (1999).
36. Hockett, P., Bisgaard, C. Z., Clarkin, O. J. & Stolow, A. Time-resolved imaging of purely valence-electron dynamics during a chemical reaction. *Nat. Phys.* **7**, 612–615 (2011).
37. Horio, T., Fuji, T., Suzuki, Y.-I. & Suzuki, T. Probing ultrafast internal conversion through conical intersection via time-energy map of photoelectron angular anisotropy. *J. Am. Chem. Soc.* **131**, 10392–10393 (2009).
38. Serrano-Pérez, J. J., González-Luque, R., Merchán, M. & Serrano-Andrés, L. On the intrinsic population of the lowest triplet state of thymine. *J. Phys. Chem. B* **111**, 11880–11883 (2007).
39. Zechmann, G. & Barbatti, M. Photophysics and deactivation pathways of thymine. *J. Phys. Chem. A* **112**, 8273–8279 (2008).
40. Neville, S. P. *et al.* Beyond structure: ultrafast X-ray absorption spectroscopy as a probe of non-adiabatic wavepacket dynamics. *Faraday Discuss.* **194**, 117–145 (2016).
41. Pertot, Y. *et al.* Time-resolved X-ray absorption spectroscopy with a water window high-harmonic source. *Science* **355**, 264–267 (2017).
42. Dell'Angela, M. *et al.* Real-time observation of surface bond breaking with an X-ray laser. *Science* **339**, 1302–1305 (2013).
43. Ekimova, M., Quevedo, W., Faubel, M., Wernet, P. & Nibbering, E. T. J. A liquid flatjet system for solution phase soft-X-ray spectroscopy. *Struct. Dyn.* **2**, 54301 (2015).
44. Mukamel, S. *et al.* Coherent multidimensional optical probes for electron correlations and exciton dynamics: from NMR to X-rays. *Acc. Chem. Res.* **42**, 553–562 (2009).
45. Dakovski, G. L. *et al.* The soft X-ray research instrument at the linac coherent light source. *J. Synchrotron Radiat.* **22**, 498–502 (2015).
46. McFarland, B. K. *et al.* Experimental strategies for optical pump-soft X-ray probe experiments at the LCLS. *J. Phys. Conf. Ser.* **488**, 12015 (2014).
47. Heimann, P. *et al.* Linac coherent light source soft X-ray materials science instrument optical design and monochromator commissioning. *Rev. Sci. Instrum.* **82**, 93104 (2011).
48. Frasiniski, L. J. *et al.* Dynamics of hollow atom formation in intense X-ray pulses probed by partial covariance mapping. *Phys. Rev. Lett.* **111**, 73002 (2013).
49. Beye, M. *et al.* X-ray pulse preserving single-shot optical cross-correlation method for improved experimental temporal resolution. *Appl. Phys. Lett.* **100**, 121108 (2012).
50. Stanton, J. F. *et al.* CFOUR coupled-cluster techniques for computational chemistry, a quantum-chemical program package. Current version available at <http://www.cfour.de>.
51. Shao, Y. *et al.* Advances in molecular quantum chemistry contained in the Q-Chem 4 program package. *Mol. Phys.* **113**, 184–215 (2015).
52. Aidas, K. *et al.* The Dalton quantum chemistry program system. *Wiley Interdiscip. Rev. Comput. Mol. Sci.* **4**, 269–284 (2014).
53. Christiansen, O., Koch, H. & Jørgensen, P. Response functions in the CC3 iterative triple excitation model. *J. Chem. Phys.* **103**, 7429–7441 (1995).
54. Koch, H., Christiansen, O., Jørgensen, P., Merás, A. M. Sde & Helgaker, T. The CC3 model: an iterative coupled cluster approach including connected triples. *J. Chem. Phys.* **106**, 1808–1818 (1997).
55. Koch, H. & Jørgensen, P. Coupled cluster response functions. *J. Chem. Phys.* **93**, 3333–3344 (1990).
56. Pedersen, T. B. & Koch, H. Coupled cluster response functions revisited. *J. Chem. Phys.* **106**, 8059–8072 (1997).
57. Stanton, J. F. & Bartlett, R. J. The equation of motion coupled-cluster method. A systematic biorthogonal approach to molecular excitation energies, transition probabilities, and excited state properties. *J. Chem. Phys.* **98**, 7029–7039 (1993).
58. Köhn, A. & Tajti, A. Can coupled-cluster theory treat conical intersections? *J. Chem. Phys.* **127**, 44105 (2007).
59. Gauss, J. & Stanton, J. F. Analytic CCSD(T) second derivatives. *Chem. Phys. Lett.* **276**, 70–77 (1997).
60. Stanton, J. F. & Gauss, J. Analytic energy gradients for the equation-of-motion coupled-cluster method: implementation and application to the HCN/HNC system. *J. Chem. Phys.* **100**, 4695–4698 (1994).

Acknowledgements

This work was supported by the AMOS program within the Chemical Sciences, Geosciences, and Biosciences Division of the Office of Basic Energy Sciences, Office of Science, U.S. Department of Energy. Parts of this research were carried out at the Linac Coherent Light Source (LCLS) at the SLAC National Accelerator Laboratory. LCLS is an Office of Science User Facility operated for the U.S. Department of Energy Office of Science by Stanford University. We thank NOTUR for computer time through Project nn2962k. M.G. acknowledges funding via the Office of Science Early Career Research Program through the Office of Basic Energy Sciences, U.S. Department of Energy and NB under Grant No. DE-SC0012376. M.G. is now funded by a Lichtenberg Professorship from the Volkswagen foundation. T.J.A.W. thanks the German National Academy of Sciences Leopoldina for a fellowship (Grant No. LPDS2013-14). H.K. acknowledges support from FP7-PEOPLE-2013-IOF (Project No. 625321). J.G. acknowledges the European Research Agency via the FP-7 PEOPLE Program (Marie Curie Action 298210). S.C. acknowledges support from the AIAS-COFUND program (Grant Agreement No. 609033). R.F. would like to acknowledge financial support from the Knut and Alice Wallenberg Foundation, Sweden, and the Swedish Research Council.

Author contributions

T.J.A.W., J.P.C., R.J.S., A.B., N.B., C.B., P.B., R.F., G.C., K.J.G., J.G., S.P.M., M.M., A.N., R.O., T.O., O.P., S.W., and M.G.: Prepared and conducted the experiment at Linac Coherent Light Source. R.H.M., S.C., and H.K.: Developed and implemented the methodology to simulate excited state NEXAFS spectra. R.H.M., S.M., and H.K.: Performed the calculations. T.J.A.W. and M.G.: Analyzed the experimental data. T.J.A.W., R.H.M., T.J.M., H.K., and M.G.: Interpreted the results and wrote the manuscript. All authors discussed the science and the paper.


Additional information

Supplementary Information accompanies this paper at doi:10.1038/s41467-017-00069-7.

Competing interests: The authors declare no competing financial interests.

Reprints and permission information is available online at <http://npg.nature.com/reprintsandpermissions/>

Publisher's note: Springer Nature remains neutral with regard to jurisdictional claims in published maps and institutional affiliations.

 **Open Access** This article is licensed under a Creative Commons Attribution 4.0 International License, which permits use, sharing, adaptation, distribution and reproduction in any medium or format, as long as you give appropriate credit to the original author(s) and the source, provide a link to the Creative Commons license, and indicate if changes were made. The images or other third party material in this article are included in the article's Creative Commons license, unless indicated otherwise in a credit line to the material. If material is not included in the article's Creative Commons license and your intended use is not permitted by statutory regulation or exceeds the permitted use, you will need to obtain permission directly from the copyright holder. To view a copy of this license, visit <http://creativecommons.org/licenses/by/4.0/>.

© The Author(s) 2017